ENERGETIC CATALYST-HYDROGEN PLASMA REACTION AS A POTENTIAL NEW ENERGY SOURCE

R. L. Mills, Y. Lu, M. Nansteel, J. He, A. Voigt, W. Good, B. Dhandapani

BlackLight Power, Inc., 493 Old Trenton Road,Cranbury, NJ 08512

Introduction

Theoretical Predictions. The basic spectral emission of pure helium and hydrogen light sources have been well known for about a century. Recently, however, unique vacuum ultraviolet (VUV) emission lines were found at predicted wavelengths and reported in numerous publications [1-5]. For example, extreme ultraviolet (EUV) spectroscopy was recorded on microwave discharges of helium with 2% hydrogen. Novel emission lines were observed with energies of $q \cdot 13.6\,eV$, $q = 1,2,3,7,9,11$. or $q \cdot 13.6\,eV$, $q = 4,6,8$ less $21.2\,eV$ corresponding to inelastic scattering of these photons by helium atoms due to excitation of $He(1s^2)$ to $He(1s^1 2p^1)$. These strong emissions are not found in any single gas plasma, and cannot be assigned to the known emission of any species of the single gases studied such as H, H^-, H_2, H_2^+, H_3^+, He, He_2^*, and He^+, known species of the mixture such as He_2^+, HeH^+, HeH, HHe_2^+, and HHe_n^+ and possible contaminants [1], or doubly excited states [6]. However the results can be explained by a novel catalytic reaction of atomic hydrogen [1-5] to lower-energy states given by Rydberg's equation

$$E_n = -\frac{e^2}{n^2 8\pi\varepsilon_o a_H} = -\frac{13.598\,eV}{n^2} \tag{1a}$$

where

$$n = \frac{1}{2}, \frac{1}{3}, \frac{1}{4}, ..., \frac{1}{p}; \quad p \le 137 \text{ is an integer} \tag{1b}$$

replaces the well known parameter

$$n = 1,2,3,... \tag{1c}$$

for hydrogen excited states.

The theory reported previously [1-5, 7-12] predicts that atomic hydrogen may undergo a catalytic reaction with certain atoms, excimers, and ions which provide a reaction with a net enthalpy of an integer multiple of the potential energy of atomic hydrogen, $E_h = 27.2\,eV$ where E_h is one hartree. Specific species (e.g. He^+, Ar^+, Sr^+, and K) identifiable on the basis of their known electron energy levels are required to be present in plasmas with atomic hydrogen to catalyze the process. In contrast, species such as atoms or ions of Kr, Xe, Na, or Mg do not fulfill the catalyst criterion—a chemical or physical process with an enthalpy change equal to an integer multiple of E_h that is sufficiently reactive with atomic hydrogen under reaction conditions. The highly exothermic reaction involves a nonradiative energy transfer followed by $q \cdot 13.6\,eV$ emission or $q \cdot 13.6\,eV$ transfer to H to form extraordinarily hot H [1, 10-16] and a hydrogen atom that is lower in energy than unreacted atomic hydrogen that corresponds to a fractional principal quantum number given by Eq. (1b). That is, the $n = 1$ state of hydrogen and the $n = \frac{1}{\text{integer}}$ states of hydrogen are nonradiative, but a transition between two nonradiative states, say $n = 1$ to $n = 1/2$, is possible via a nonradiative energy transfer. A catalyst provides a net positive enthalpy of reaction of $m \cdot 27.2\,eV$ (i.e. it resonantly accepts the nonradiative energy transfer from hydrogen atoms and releases the energy to the surroundings to affect electronic transitions to fractional quantum energy levels). As a consequence of the nonradiative energy transfer, the hydrogen atom becomes unstable and emits further energy until it achieves a lower-energy nonradiative state having a principal energy level given by Eqs. (1a) and (1b).

Prior related studies that support the possibility of a novel reaction of atomic hydrogen which produces hydrogen in fractional quantum states that are at lower energies than the traditional "ground" ($n = 1$) state include extreme ultraviolet (EUV) spectroscopy [1-5, 9-12, 15, 17-24, 26-28], characteristic emission from catalysts and the hydride ion products [11-12, 17-20, 23-24], lower-energy hydrogen emission [1-5], chemically formed plasmas [9-12, 17-24], Balmer α line broadening [1, 2, 10-17, 20, 23-24, 26-27], population inversion of H lines [23-26], elevated electron temperature [13-15, 27], anomalous plasma afterglow duration [21-22], power generation [2, 4, 15, 20, 27, 29], and analysis of novel chemical compounds [20, 30-33].

$H(1/p)$ may react with a proton, and two $H(1/p)$ may react to form $H_2(1/p)^+$ and $H_2(1/p)$, respectively. The hydrogen molecular ion and molecular charge and current density functions, bond distances, and energies were solved previously [8] from the Laplacian in ellipsoidal coordinates with the constraint of nonradiation. The bond dissociation energy, E_D, of hydrogen molecular ion $H_2(1/p)^+$ was given as

$$E_D = p^2 2.535\,eV + p^3 0.118755\,eV \tag{2}$$

where p is an integer. The bond dissociation energy, E_D, of hydrogen molecule $H_2(1/p)$ E_D was given previously as

$$E_D = p^2 4.151\,eV + p^3 0.326469\,eV \tag{3}$$

The vibrational and rotational energies of fractional-Rydberg-state hydrogen molecular ion $H_2(1/p)^+$ and molecular hydrogen $H_2(1/p)$ are p^2 those of H_2^+ and H_2, respectively. Thus, the vibrational energies, E_{vib}, for the $\upsilon = 0$ to $\upsilon = 1$ transition of hydrogen-type molecular ions $H_2(1/p)^+$ are [8]

$$E_{vib} = p^2 0.271\,eV \tag{4}$$

where p is an integer and the experimental vibrational energy for the $\upsilon = 0$ to $\upsilon = 1$ transition of H_2^+, $E_{H_2^+(\upsilon=0\to\upsilon=1)}$, is given by Karplus and Porter [34] and NIST [35]. Similarly, the vibrational energies, E_{vib}, for the $\upsilon = 0$ to $\upsilon = 1$ transition of hydrogen-type molecules $H_2(1/p)$ are [8]

$$E_{vib} = p^2 0.515902\,eV \tag{5}$$

where p is an integer and the experimental vibrational energy for the $\upsilon = 0$ to $\upsilon = 1$ transition of H_2, $E_{H_2(\upsilon=0\to\upsilon=1)}$, is given by Beutler [36] and Herzberg [37]. The rotational energies, E_{rot}, for the J to $J+1$ transition of hydrogen-type molecules $H_2(1/p)$ are [8]

$$E_{rot} = E_{J+1} - E_J = \frac{\hbar^2}{I}[J+1] = p^2(J+1)0.01509\,eV \tag{6}$$

where p is an integer, I is the moment of inertia, and the experimental rotational energy for the $J=0$ to $J=1$ transition of H_2 is given by Atkins [38]. The p^2 dependence of the rotational energies results from an inverse p dependence of the internuclear distance and the corresponding impact on I. The predicted internuclear distances $2c'$ for $H_2(1/p)$ are

$$2c' = \frac{a_o\sqrt{2}}{p} \tag{7}$$

Experiments to Test the Theoretical Predictions. The reaction Ar^+ to Ar^{2+} has a net enthalpy of reaction of $27.63\,eV$; thus, it may serve as a catalyst to form $H(1/2)$. The product of the catalysis reaction, $H(1/2)$, may further serve as both a catalyst and a reactant to form $H(1/4)$ [2-3]. Also, the second ionization energy of helium is $54.4\,eV$; thus, the ionization reaction of He^+ to He^{2+} has a net enthalpy of reaction of $54.4\,eV$ which is equivalent to $2\cdot 27.2\,eV$. The product of the catalysis reaction, $H(1/3)$, may further serve as both a catalyst and a reactant to form $H(1/4)$ and $H(1/2)$ [2-3].

Since $H_2(1/2)^+$ is a resonant state of $H_2(1/4)^+$, the reaction designated

$$H(1/4)+H^+ \rightarrow H_2(1/4)^+ \tag{8}$$

wherein $H(1/4)$ reacts with a proton to form $H_2(1/4)^+$ is possible with strong emission through vibronic coupling with the resonant state $H_2(1/2)^+$. The energies, E_{D+vib}, of this series due to vibration in the transition state given previously [28] are

$$\begin{aligned} E_{D+vib} &= E_D\left(H_2(1/4)^+\right) - \left(\upsilon^* + \frac{1}{2}\right)2^2 E_{vib\,H_2^+} \\ &= 48.16 - \left(\upsilon^* + \frac{1}{2}\right)1.172\,eV \end{aligned}, \quad \upsilon^* = 0,1,2,3... \tag{9}$$

where $E_D\left(H_2(1/4)^+\right)$ is the bond energy of $H_2(1/4)^+$ given by Eq. (2) and $E_{vib\,H_2^+}$ is the transition-state vibrational energy of H_2^+ given by Eq. (108) of Ref. [8]. In Eq. (9), υ^* refers to vibrational energies of the transition state which must have equal energy separation as a requirement for resonant emission [8, 28]. Thus, anharmonicity is not predicted. The series is predicted to end at 25.74 nm corresponding to the predicted $H_2(1/4)^+$ bond energy of 48.16 eV given by Eq. (2).

The present paper tests theoretical predictions [1-5, 7-12] that atomic and molecular hydrogen form stable states of lower energy than traditionally thought possible. Substantial spectroscopic and physical differences are anticipated. For example, novel EUV atomic, molecular ion, and molecular spectral emission lines from transitions corresponding to energy levels given by Eqs. (1a) and (1b), Eqs. (2) and (4), and Eqs. (3) and (5-7), respectively, are predicted. The atomic lines have been shown previously [1-4, 27] as well as a series of unique EUV lines assigned to $H_2(1/2)$ [4]. To test additional predictions, EUV spectroscopy was performed to search for emission that was characteristic of and identified $H_2(1/4)^+$ and $H_2(1/4)$. Low pressure plasmas are more highly ionized. Thus, we further investigated the emission of the $H_2(1/4)^+$ vibrational series given by Eq. (9) from microwave discharges of helium-hydrogen and argon-hydrogen mixtures.

The rotational energies provide a very precise measure of I and the internuclear distance using well established theory [34]. Neutral molecular emission was anticipated for high pressure argon-hydrogen plasmas excited by a 15 keV electron beam. Rotational lines for $H_2(1/4)$ were anticipated and sought in the 150-250 nm region. The spectral lines were compared to those predicted by Eqs. (5-6) corresponding to the internuclear distance of 1/4 that of H_2 given by Eq. (7). The predicted energies for the $\upsilon=1\rightarrow\upsilon=0$ vibration-rotational series of $H_2(1/4)$ (Eqs. (5-6)) are

$$\begin{aligned} E_{vib-rot} &= p^2 E_{vib\,H_2(\upsilon=0\rightarrow\upsilon=1)} \pm p^2(J+1)E_{rot\,H_2} \\ &= 4^2 E_{vib\,H_2(\upsilon=0\rightarrow\upsilon=1)} \pm 4^2(J+1)E_{rot\,H_2} \\ &= 8.254432\,eV \pm (J+1)0.24144\,eV \end{aligned}, \quad J = 0,1,2,3... \tag{10}$$

for $p=4$.

The product $H_2(1/p)$ gas predicted to liquefaction at a higher temperature than H_2 [28]. Helium-hydrogen (90/10%) plasma gases were flowed through a high-vacuum (10^{-6} Torr) capable, liquid nitrogen (LN) cryotrap, and the condensed gas was characterized by ^1H nuclear magnetic resonance (NMR) of the LN-condensable gas dissolved in $CDCl_3$. Other sources of hydrogen such as hydrocarbons were eliminated by mass spectroscopy (MS) and Fourier transform infrared spectroscopy (FTIR). The ^1H NMR resonance of $H_2(1/p)$ is predicted to be upfield from that of H_2 due to the fractional radius in elliptic coordinates [7-8] wherein the electrons are significantly closer to the nuclei. The predicted shift, $\frac{\Delta B_T}{B}$, for $H_2(1/p)$ derived previously [7-8] is given by the sum of that of H_2 and a relativistic term that depends on $p>1$:

$$\frac{\Delta B_T}{B} = -\mu_0\left(4-\sqrt{2}\ln\frac{\sqrt{2}+1}{\sqrt{2}-1}\right)\frac{e^2}{36a_0 m_e}\left(1+\pi\alpha(p-1)\right) \tag{11}$$

$$\frac{\Delta B_T}{B} = -\left(28.01+0.64(p-1)\right)ppm \tag{12}$$

where for H_2 there is no relativistic effect and $p=\text{integer}>1$ for $H_2(1/p)$.

The exothermic helium plasma catalysis of atomic hydrogen was shown previously [13-14] by the observation of an average hydrogen atom temperature of $180\text{-}210\,eV$ for helium-hydrogen mixed plasmas versus $\approx 3\,eV$ for hydrogen alone. Since the electronic transitions are very energetic, power balances of helium-hydrogen plasmas compared to control krypton plasmas were measured using water bath calorimetry to determine whether this reaction has sufficient kinetics to merit its consideration as a practical power source.

$2K^+$ to $K+K^{2+}$ and K to K^{3+} also provide a reaction with a net enthalpy equal to one and three times the potential energy of atomic hydrogen, respectively. The presence of these gaseous ions or atoms with thermally dissociated hydrogen formed a so-called resonance transfer (rt)-plasma having strong VUV emission with a stationary inverted Lyman population [9, 17, 19-24]. Significant line broadening of the Balmer α, β, and γ lines of 18 eV was observed, compared to 3-4 eV from a hydrogen microwave plasma

[17, 23-24]. Emission from rt-plasmas occurred even when the electric field applied to the plasma was zero [21-22]. Light output per unit power input up to 8600 times that of the control standard light sources as also observed from certain rt-plasmas [10-12]. The reaction was exothermic since excess power of 20 $mW \cdot cm^{-3}$ was measured by Calvet calorimetry [20]. An energetic catalytic reaction was proposed involving a resonant energy transfer between hydrogen atoms and $2K^+$ or K to form very stable novel hydride ions $H^-(1/p)$ called hydrino hydrides having a fractional principal quantum numbers $p = 2$ and $p = 4$, respectively. Characteristic emission was observed from K^{2+} and K^{3+} that confirmed the resonant nonradiative energy transfer of $27.2\,eV$ and $3 \cdot 27.2\,eV$ from atomic hydrogen to $2K^+$ and K, respectively. The product hydride ion $H^-(1/4)$ was observed spectroscopically at $110\,nm$ corresponding to its predicted binding energy of $11.2\,eV$ [17, 19, 20].

In addition to liquefaction at liquid nitrogen temperature, $H_2(1/p)$ gas was also isolated by decomposition of compounds found to contain the corresponding hydride ions $H^-(1/p)$. The total shift, $\frac{\Delta B_T}{B}$, was calculated previously [6, 20] for the hydride ions $H^-(1/p)$ having a fractional principal quantum number. The shift was given by the sum of that of ordinary hydride ion H^- and a component due to a relativistic effect:

$$\begin{aligned}\frac{\Delta B_T}{B} &= -\mu_0 \frac{e^2}{12 m_e a_0 \left(1+\sqrt{s(s+1)}\right)}\left(1+\alpha 2\pi(p-1)\right) \\ &= -\left(29.9 + 1.37(p-1)\right) ppm\end{aligned} \tag{13}$$

where for H^- there is no relativistic effect and $p = \text{integer} > 1$ for $H^-(1/p)$. The experimental absolute resonance shift of tetramethylsilane (TMS) is -31.5 ppm relative to the proton's gyromagnetic frequency [39, 40]. The results of ^1H MAS NMR spectroscopy were given previously [20, 31-32] on control and novel hydrides synthesized using atomic potassium as a hydrogen catalyst wherein the triple ionization reaction of K to K^{3+}, has a net enthalpy of reaction of $81.7766\,eV$, which is equivalent to $3 \cdot 27.2\,eV$. The KH experimental shift of +1.3 ppm relative to TMS corresponding to absolute resonance shift of -30.2 ppm matched very well the predicted shift of H^- of -30 ppm given by Eq. (13). The ^1H MAS NMR spectrum of novel compound $KH*Cl$ relative to external tetramethylsilane (TMS) showed a large distinct upfield resonance at -4.4 ppm corresponding to an absolute resonance shift of -35.9 ppm that matched the theoretical prediction of p = 4. A novel peak of $KH*I$ at -1.5 ppm relative to TMS corresponding to an absolute resonance shift of -33.0 ppm matched the theoretical prediction of p = 2. The predicted catalyst reactions, position of the upfield-shifted NMR peaks, and spectroscopic data for $H^-(1/2)$ and $H^-(1/4)$ were found to be in agreement [7, 20].

The decomposition reaction of $H^-(1/p)$ is

$$2M^+H^-(1/p) \xrightarrow{\Delta} H_2(1/p) + 2M \tag{14}$$

where M^+ is a metal ion. NMR peaks of $H_2(1/p)$ given by Eqs. (11-12) provide a direct test of whether compounds such as $KH*I$ contain hydride ions in the same fractional quantum state p. Furthermore, the observation of a series of singlet peaks upfield of H_2 with a predicted integer spacing of 0.64 ppm provides a powerful means to confirm the existence of $H_2(1/p)$.

Since atomic hydrogen and K atoms are formed by reduction at the cathode of an aqueous K_2CO_3 electrolysis cell and K^+ ions present in the electrolyte as well as the K atoms contact the atomic hydrogen at the cathode, the catalysis of atomic hydrogen to fractional Rydberg states was also predicted to occur in these cells. The electrolysis reaction is supported by the observation of novel hydride compounds that were reported previously [33]. For example, after 10^4 hours of continuous aqueous electrolysis with K_2CO_3 as the electrolyte, highly stable novel inorganic hydride compounds such as $KH\,KHCO_3$ and KH were isolated and identified by time of flight secondary ion mass spectroscopy (ToF-SIMS). The existence of novel hydride ions was determined using X-ray photoelectron spectroscopy (XPS) and ^1H MAS NMR.

The energy given off during catalysis is much greater than the energy initially transferred to the catalyst, and the energy released is large as compared to conventional chemical reactions. For example, when hydrogen and oxygen gases undergo combustion to form water

$$H_2(g) + \frac{1}{2}O_2(g) \rightarrow H_2O(l) \tag{15}$$

the known enthalpy of formation of water is $\Delta H_f = -286\,kJ/mole$ or 1.48 eV per hydrogen atom. By contrast, each ($n = 1$) ordinary hydrogen atom undergoing a catalysis step to $n = \frac{1}{2}$ releases a net of $40.8\,eV$. Moreover, further catalytic transitions may occur: $n = \frac{1}{2} \rightarrow \frac{1}{3}, \frac{1}{3} \rightarrow \frac{1}{4}, \frac{1}{4} \rightarrow \frac{1}{5}$, and so on. Once catalysis begins, $H(1/p)$ atoms autocatalyze further in a process called disproportionation discussed previously [2-3, 7].

The power corresponding to the exothermic reaction to form H states given by Eqs. (1a) and (1b) was studied by measuring the temperature of the electrolyte of a K_2CO_3 electrolytic cell for a given input electrolysis power compared to the heat loss of the electrolyte using a resistive heater. For sodium, no electrocatalytic reaction of approximately $27.2\,eV$ is possible by the transfer of an electron between two Na^+ ions as is the case with K^+. Thus, Na_2CO_3 served as a control electrolyte. $H_2(1/p)$ formed from the product $H(1/p)$ has an internuclear distance of $1/p$ times that of H_2; thus, it is predicted to have a higher mobility through metals than H_2. This provided a means to enrich and isolate $H_2(1/p)$ by differential diffusion through a hollow nickel cathode. The collected gas was dissolved in dissolved in $CDCl_3$ and characterized by ^1H NMR which has the capability to measure the energy state of hydrogen according to Eqs. (11-12) with the elimination of hydrocarbons as the source of the peaks by FTIR. Since the ionization energy of $H_2(1/2)$ is about a factor of four times that of H_2 ($IP_1(H_2(1/2)) = 62.53\,eV$ versus $IP_1(H_2) = 15.426\,eV$) [7-8, 28], the mass spectral $m/e = 2$ ion current as a function of time was recorded while changing the

electron gun energy from 30 to 70 eV for ultrapure hydrogen and the gas collected electrolysis gases.

Experimental

To investigate the vibrational series of $H_2(1/4)^+$, EUV spectra (20-65 nm) were recorded on light emitted from microwave discharge plasmas of helium, argon, krypton, or xenon or a mixture of 10% hydrogen with each noble gas. Each ultrapure (99.999+%) test gas or mixture was flowed through a half inch diameter quartz tube at 100 mTorr maintained with a total gas flow rate of 10 sccm. The tube was fitted with an Opthos coaxial microwave cavity (Evenson cavity). The microwave generator was an Opthos Model MPG-4M generator (Frequency: 2450 MHz). The input power to the plasma was set at 40 W.

The spectrometer was a McPherson 4° grazing incidence EUV spectrometer (Model 248/310G) equipped with a grating having 600 G/mm with a radius of curvature of $\approx 1\,m$ that covered the region $5-65\,nm$. The angle of incidence was 87°. The wavelength resolution was about $0.1\,nm$ (FWHM) with an entrance and exit slit width of $40\,\mu m$. A CEM was used to detect the EUV light. The increment was $0.01\,nm$ and the dwell time was $1\,s$.

Vibration-rotational emission of $H_2(1/4)$ was investigated using an electron gun described previously [41, 42] to initiate argon plasmas with 1% hydrogen in the pressure range of 450-1000 Torr. The plasma cell was flushed with oxygen, then pumped down, flushed with argon-hydrogen (99/1%), and filled with argon-hydrogen (99/1%). Krypton replaced argon in the controls, and argon, hydrogen, oxygen, nitrogen, water vapor, nitrogen-oxygen (50/50%), and argon or krypton with oxygen addition up to 100% oxygen served as further controls. The Ar^+ catalyst mechanism was tested by atmospheric-pressure-plasma-gas flow at 75 sccm and nonflow conditions. The electrons were accelerated with a high voltage of 12.5 keV at a beam current of $10\,\mu A$. The electron gun was sealed with a thin (300 nm thickness) SiN_x foil that served as a $1\ mm^2$ electron window to the cell at high gas pressure (760 Torr). The beam energy was deposited by hitting the target gases, and the light emitted by beam excitation exited the cell through a MgF_2 window mounted at the entrance of a normal incidence McPherson 0.2 meter monochromator (Model 302) equipped with a 1200 lines/mm holographic grating with a platinum coating. The resolution was $0.5\,nm$ (FWHM) at an entrance and exit slit width of $100\,\mu m$. The increment was $0.1\,nm$ and the dwell time was $1\,s$. The PMT (Model R8486, Hamamatsu) used has a spectral response in the range of 115-320 nm with a peak efficiency at about 225 nm. The emission was essentially flat for $200 < \lambda > 275\,nm$, but a notch in the response of about 20% existed in the short wavelength range with a minimum at 150 nm. Peak assignments were determined by an external calibration against standard line emissions.

Condensable gas from helium-hydrogen (90/10%) microwave plasmas maintained in the Evenson cavity was collected in a high-vacuum (10^{-6} Torr) capable, LN cryotrap described previously [28]. After each plasma run the cryotrap was pumped down to 10^{-5} Torr to remove any non-condensable gases in the system. The pressure was recorded as a function of time as the cryotrap was warmed to room temperature. Typically, about $45\,\mu moles$ of condensed gas was collected in a 2 hr plasma run. Controls were hydrogen and helium alone.

The mass spectra ($m/e = 1$ to $m/e = 200$) of ultrahigh purity (99.999+%) hydrogen (Praxair) control samples and samples of the condensable gas from the helium-hydrogen microwave plasmas were recorded with a residual gas analyzer.

Premixed He/H_2 (90/10%) was flowed from a supply bottle through a metering valve and a LN trap just upstream of a 700 mTorr Evenson microwave plasma. A second LN trap downstream of the plasma tube was used to remove any water vapor generated by the plasma. The plasma gas, devoid of impurities due to the LN traps, was flowed through a long capillary tube which was maintained in the temperature range ~12-17 K by a cryo-cooler described previously [28]. Residual gas was pumped from the capillary, condensable gas was collected over a period of several hours, and the system was evacuated to 10^{-5} Torr to remove any non-condensable gases in the system. Controls were hydrogen and helium alone. Two capillary valves were closed to trap any vaporizing gas as the cryo-cooler was stopped, and the tube was warmed to room temperature. Typically about 100 mTorr of gas was collected over a 24 to 48 hour period and then analyzed by mass spectroscopy and compared with the results for a control sample collected in the same way, except that no plasma was present.

Sealed ^1H NMR samples were prepared by collecting the condensed gas from the cryotrap in $CDCl_3$ solvent (99.99% Cambridge isotopes) in an NMR tube (5 mm OD, 23 cm length, Wilmad) maintained at LN-temperature which was then sealed as described previously [28]. Control NMR samples comprised ultrahigh purity hydrogen (Praxair) and the helium-hydrogen (90/10%) mixture with $CDCl_3$ solvent. The NMR spectra were recorded with a 300 MHz Bruker NMR spectrometer that was deuterium locked. The chemical shifts were referenced to the frequency of tetramethylsilane (TMS) at 0.00 ppm.

$KH*I$ that was prepared under long duration (two weeks) synthesis according to methods given previously [30-32], and about a one gram sample was placed in a thermal decomposition reactor under an argon atmosphere. The reactor comprised a 1/4" OD by 3" long quartz tube that was sealed at one end and connected at the open end with Swagelock™ fittings to a T. One end of the T was connected to the NMR tube containing $CDCl_3$ solvent, and the other end was attached to a turbo pump. The apparatus was evacuated to less than 1 milliTorr with the $CDCl_3$ maintained at LN temperature. The sample was heated to 200 °C under vacuum. A valve to the pump was closed, and the sample was heated in the evacuated quartz chamber containing the sample to above 600 °C until the sample melted. Gas released from the sample was collected in the $CDCl_3$ solvent, the NMR tube was sealed and warmed to room temperature, and the NMR spectrum was recorded. Using identical samples, the NMR-tube end of the collection apparatus was connected directly to the sampling port of a quadrupole mass spectrometer to test for hydrocarbon contamination. FTIR was also performed on the released gas for this purpose.

An NMR sample from $KH*I$ provided by BlackLight Power, Inc. was also prepared and analyzed at the Naval Air Warfare Center Weapons Division, Naval Air Warfare Center, China Lake, CA under the same procedure except that the $CDCl_3$ solvent was maintained at ice temperature during hydrogen gas collection, and the NMR spectrum was recorded with a 400 MHz instrument at China Lake. Control NMR samples of ultrapure hydrogen dissolved in $CDCl_3$ solvent were also prepared, and NMR spectra were

obtained under conditions matching those of the $KH*I$ -derived samples.

The excess power was measured by water bath calorimetry on helium-hydrogen (95/5%) plasmas maintained in a microwave discharge cell compared to control plasmas with the same input power as described previously [27]. The water bath was calibrated by a high precision heater and power supply. A high precision linear response thermistor probe (Omega OL-703) recorded the temperature of the 45 L water bath as a function of time for the stirrer alone to establish the baseline. The heat capacity was determined for several input powers, 30, 40, and 50 W ± 0.01 W, and was found to be independent of input power over this power range within ± 0.05%. The temperature rise of the reservoir as a function of time gave a slope in °C/s. This slope was baseline corrected for the negligible stirrer power and loss to ambient. The constant known input power (J/s), was divided by this slope to give the heat capacity in J/°C. Then, in general, the total power output from the cell to the reservoir was determined by multiplying the heat capacity by the rate of temperature rise (°C/s) to give J/s.

Since the cell and water bath system were adiabatic, the general form of the power balance equation with the possibility of excess power is:

$$P_{in} + P_{ex} - P_{out} = 0 \tag{16}$$

where P_{in} is the microwave input power, P_{ex} is the excess power generated from the hydrogen catalysis reaction, and P_{out} is the thermal power loss from the cell to the water bath. Since the cell was surrounded by water that was contained in an insulated reservoir with negligible thermal losses, the temperature response of the thermistor T as a function of time t was determined to be

$$\dot{T}(t) = \left(1.940\ X\ 10^5\ J/°C\right)^{-1} \times P_{out} \tag{17}$$

where $1.940\ X\ 10^5\ J/°C$ is the heat capacity for the least square curve fit of the response to power input for the control experiments ($P_{ex} = 0$). The slope was recorded for about 2 hours after the cell had reached a thermal steady state, to achieve an accuracy of ± 1%.

The power balance of the electrolysis of aqueous potassium carbonate (K^+/K^+ and K catalysts) was determined using single cell 350 ml silvered vacuum jacketed dewars and compared with the results with the replacement of K_2CO_3 with Na_2CO_3 as described previously [29]. A linear calibration curve was obtained. Two methods of differential calorimetry were used to determine the cell constant which was used to calculate the excess enthalpy. First, the cell constant was calculated during the experiment (on-the-fly-calibration) by turning an internal resistance heater off and on, and inferring the cell constant from the difference between the losses with and without the heater. Second, the cell constant was determined with no electrolysis processes occurring by turning an internal resistance heater off and on for a well stirred matched dewar cell, and inferring the cell constant from the difference between the losses with and without the heater.

The general form of the energy balance equation for the cell in steady state is:

$$0 = P_{appl} + Q_{htr} + Q_{xs} - P_{gas} - Q_{loss} \tag{18}$$

where P_{appl} is the electrolysis power; Q_{htr} is the power input to the heater; Q_{xs} is the excess heat power generated by the hydrogen catalysis reaction; P_{gas} is the power removed as a result of evolution of H_2 and O_2 gases; and Q_{loss} is the thermal power loss from the cell. When an aqueous solution is electrolyzed to liberate hydrogen and oxygen gasses, the electrolysis power $P_{appl}\,(= E_{appl} I)$ can be partitioned into two terms:

$$P_{appl} = E_{appl} I = P_{cell} + P_{gas} \tag{19}$$

An expression for $P_{gas}\left(= E_{gas} I\right)$ is readily obtained from the known enthalpy of formation of water from its elements:

$$E_{gas} = \frac{-\Delta H_{form}}{\alpha F} \tag{20}$$

(F is Faraday's constant), which yields $E_{gas} = 1.48V$ for the reaction

$$H_2O \rightarrow H_2 + \frac{1}{2} O_2 \tag{21}$$

The net Faradaic efficiency of gas evolution is assumed to be unity; thus, Eq. (19) becomes

$$P_{cell} = (E_{appl} - 1.48V)I \tag{22}$$

The cell was calibrated for heat losses by turning an internal resistance heater off and on while maintaining constant electrolysis and by inferring the cell conductive constant from the difference between the losses with and without the heater where heat losses were primarily conductive losses through the cap of the dewar. When the heater was off, the losses were given by

$$c(T_c - T_b) = P_{appl} + 0 + Q_{xs} - P_{gas} \tag{23}$$

where c is the conductive heat loss coefficient; T_b is ambient temperature and T_c is the cell temperature. When a new steady state is established with the heater on, the losses change to:

$$c(T_c' - T_b) = P'_{appl} + Q_{htr} + Q'_{xs} - P'_{gas} \tag{24}$$

where a prime superscript indicates a changed value when the heater was on. When the following assumptions apply

$$Q_{xs} = Q'_{xs}\ ;\ P_{appl} = P'_{appl}\ ;\ P_{gas} = P'_{gas} \tag{25}$$

the cell constant or heating coefficient a, the reciprocal of the conductive loss coefficient (c), is given by the result

$$a = \frac{T_c' - T_c}{Q_{htr}} \tag{26}$$

In all heater power calculations, the following equation was used

$$Q_{htr} = E_{htr} I_{htr} \tag{27}$$

The experiments were carried out by observing and comparing the temperature difference ($\Delta T_1 = T(electrolysis\ only) - T(blank)$) and ($\Delta T_2 = T(resistor\ heating\ only) - T(blank)$) referred to unit input power, between two identical dewars. The heating coefficients were calculated from

$$a_1 = \frac{\Delta T_1}{P_{cell}} \tag{28}$$

$$a_2 = \frac{\Delta T_2}{Q_{htr}} \tag{29}$$

Then, the excess power is given by

$$Q_{xs} = \frac{\Delta T_1}{a_2} - P_{cell} \tag{30}$$

or

$$Q_{xs} = P_{cell}\left(\frac{a_1}{a_2} - 1\right) \tag{31}$$

The heating coefficient was also determined "on the fly" by the addition of increments of ~0.1 W of heater power to the electrolytic cell where 24 hours was allowed for steady state to be achieved.

The temperature rise above ambient ($\Delta T_3 = T(electrolysis + heater) - T(blank)$) was recorded as well as the electrolysis power and heater power. The heating coefficient, a_3, in this case was given by the slope of the plot of ΔT_3 versus total input power ($P_{cell} + Q_{htr}$):

$$a_3 = \frac{\Delta T_3}{P_{cell} + Q_{htr}} \tag{32}$$

wherein the electrolysis heating power, P_{cell}, was kept constant. The heating coefficient a_3 and the temperature rise of the cell with electrolysis power only, ΔT_1, were used to determine the total cell power comprising $P_{cell} + Q_{xs}$. Then, Q_{xs} was determined by subtracting P_{cell}:

$$Q_{xs} = \frac{\Delta T_1}{a_3} - P_{cell} \tag{33}$$

The electrolyte solution was 200 ml of 0.57 M aqueous K_2CO_3 (Aldrich $K_2CO_3 \cdot 3/2H_2O$ 99±%) or 200 ml of 0.57 M aqueous Na_2CO_3 (Aldrich Na_2CO_3 A.C.S. primary standard 99.95 ±%).

The cathode and anode comprised 24 meters of 0.38 mm diameter coiled nickel wire (99.8 % Alfa, cold drawn, clean Ni wire). The electrodes were cleaned by placing them in a beaker of 0.57 M K_2CO_3/3% H_2O_2 for 30 minutes and then rinsing it with distilled water. The leads were inserted into Teflon tubes to insure that no recombination of the evolving gases occurred. The Faraday efficiency was determined by measuring the volume of the evolved electrolysis gases. The power was applied as 83.0 mA constant current at a measured 1.95 V. When Na_2CO_3 replaced K_2CO_3 the power was applied as 83.0 mA constant current at a measured 3.26 V.

For heat measurement and electrolysis gas collection, the cathode comprised a 170 cm long nickel tubing cathode (Ni 200 tubing, 0.159 cm O.D., 0.107 cm I.D., with a nominal wall thickness of 0.0254 cm, MicroGroup, Inc., Medway, MA). The cathode was coiled into a 3.0 cm long helix with a 2.0 cm diameter about the central Pt anode. The cathode was cleaned by placing it in a beaker of 0.57 M K_2CO_3/3% H_2O_2 for 30 minutes and then rinsing it with distilled water. The power was applied as 101 mA constant current at a measured 1.86 V. The anode was a platinum basket (Johnson Matthey) with a 0.38 mm Ni lead wire. The leads were inserted into Teflon tubes to prevent recombination, if any, of the evolving gases. The cathode-anode separation distance was 1 cm.

An ultrahigh-vacuum system was used to collected sealed ^1H NMR samples of the electrolysis gases from the hollow as described previously [29]. The NMR spectra were recorded with the 300 MHz Bruker NMR spectrometer that was deuterium locked. The chemical shifts were referenced to the frequency of tetramethylsilane (TMS) at 0.00 ppm. Hydrocarbon contamination in the samples was eliminated by mass spectroscopic analysis and by FTIR spectral analysis.

The mass spectra ($m/e = 1$ to $m/e = 200$) of ultrahigh purity hydrogen (Praxair) control samples and samples of the electrolysis gases collected in the hollow nickel cathode from K_2CO_3 and Na_2CO_3 cells were recorded with a residual gas analyzer. In addition, the ion current as a function of time of the mass to charge ratio of two ($m/e = 2$) was recorded while changing the electron gun energy from 30 to 70 eV for ultrapure hydrogen and the electrolysis gas from the hollow cathode connected directly to a needle valve on the sampling port mass spectrometer. The pressure of the sample gas in the mass spectrometer was kept the same for each experiment by adjusting the needle value of the mass spectrometer. The entire range of masses through $m/e = 200$ was measured before and after the determinations at $m/e = 1$ and $m/e = 2$.

Results and Discussion

EUV spectroscopy of Helium-Hydrogen and Argon-Hydrogen Plasmas. *Detection of Fractional Rydberg State Hydrogen Molecular Ion* $\mathbf{H_2(1/4)^+}$. In the case of the EUV spectra of helium, krypton, xenon, krypton-hydrogen (90/10%), or xenon-hydrogen (90/10%), no peaks were observed below 65 nm, and no spurious peaks or artifacts due to the grating or the spectrometer were observed. No changes in the emission spectra were observed by the addition of hydrogen to noncatalysts krypton or xenon. Only known atom and ion peaks were observed in the EUV spectrum of the helium and argon microwave discharge emission.

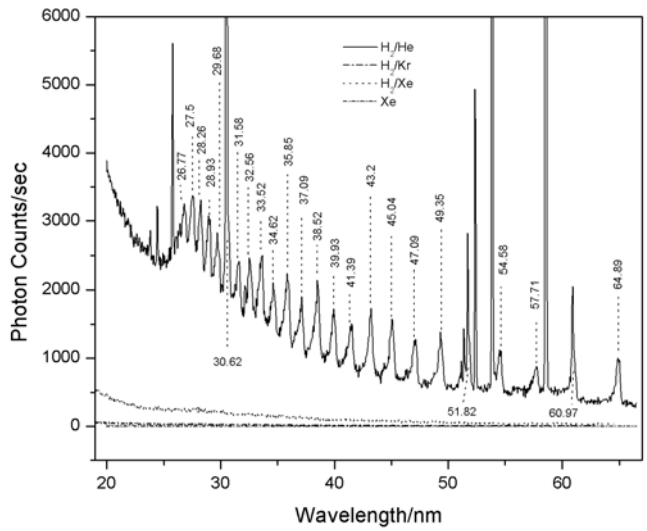

Figure 1. The EUV spectra (20-65 nm) of microwave plasmas of xenon and 10% hydrogen mixed with helium, krypton, and xenon. A vibrational pattern of peaks with an energy spacing of 1.18 eV was observed from the helium-hydrogen plasma having He^+ catalyst. The peaks matched Eq. (9) for $\upsilon^* = 0,1,2,3...24$. The series terminated at about 25.7 nm corresponding to the predicted bond energy of $H_2(1/4)^+$ of 48.16 eV given by Eq. (2). No emission was observed from the noncatalyst controls, krypton and xenon alone or with hydrogen. The sharp peaks in the spectrum were assigned to He I and He II.

The EUV spectra (20-65 nm) of the microwave plasmas of xenon and 10% hydrogen mixed with helium, krypton, and xenon are shown in Figure 1. No emission was observed from the noncatalyst controls, krypton and xenon. A characteristic vibrational series was observed for helium-hydrogen (90/10%), but at higher energies than any known molecule by about an order of magnitude. The series was not observed with helium alone as shown in Figure 2. The energies of the peaks observed in Figures 1 and 2 are plotted in Figure 3 as a function of peak number or integer υ^*. The slope of the linear curve fit in Figure 3 is 1.18 eV, and the intercept is 47.6 eV which matches the predicted series given by Eq.

(9) to within the spectrometer resolution of 1%. This energy separation matches the transition-state vibrational energy of the resonant state $H_2(1/2)^+$, and the series terminates at about 25.7 nm corresponding to the predicted bond energy of $H_2(1/4)^+$ of 48.16 eV given by Eq. (2). Thus, emission in this region was due to the reaction $H(1/4)+H^+ \rightarrow H_2(1/4)^+$ with vibronic coupling with the resonant state $H_2(1/2)^+$ within the transition state. The predicted emission at $E_{D+vib} = E_D\left(H_2(1/4)^+\right) - \left(\upsilon^* + \frac{1}{2}\right)2^2 E_{vib\,H_2^+}$ was observed for $\upsilon^* = 0,1,2,3...24$. All other peaks in the spectra were assigned to He I and He II.

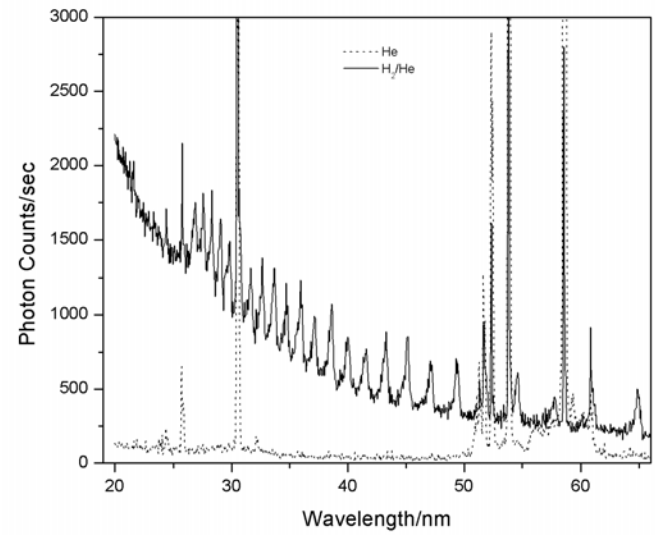

Figure 2. The EUV spectra (20-65 nm) of microwave plasmas of helium-hydrogen (90/10%) (solid) and helium alone (dashed). The vibrational series of peaks assigned to the reaction $H(1/4)+H^+ \rightarrow H_2(1/4)^+$ was observed from the helium-hydrogen plasma having He^+ catalyst and hydrogen, but not from helium alone. The sharp peaks in the spectrum were assigned to He I and He II.

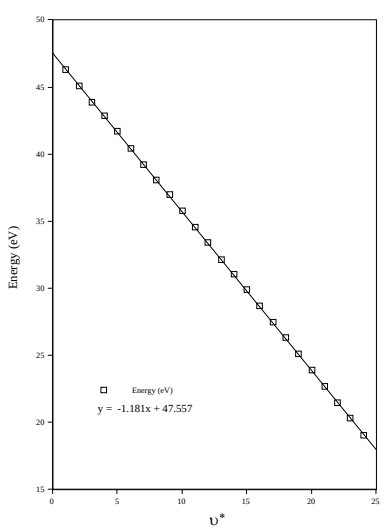

Figure 3. The plot of the energies of the peaks shown in Figures 1 and 2. The slope of the linear curve fit is 1.18 eV, and the intercept is 47.6 eV which matches the predicted emission given by Eq. (9) to within the spectrometer resolution of about 1%.

The EUV spectra (20-65 nm) of microwave plasmas of argon-hydrogen (90/10%) compared with argon alone are shown in Figure 4. The vibrational series of peaks with an energy spacing of 1.18 eV was observed from the argon-hydrogen plasma having Ar^+ catalyst with hydrogen. In contrast, the series was not observed without hydrogen. The peaks matched Eq. (9) for $\upsilon^* = 0,1,2,3...24$.

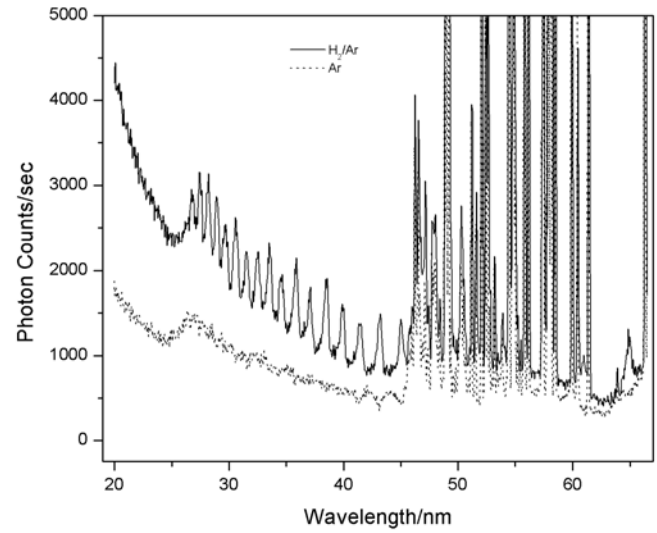

Figure 4. The EUV spectra (20-65 nm) of microwave plasmas of argon-hydrogen (90/10%) (solid) and argon alone (dashed). The vibrational series of peaks assigned to the reaction $H(1/4)+H^+ \rightarrow H_2(1/4)^+$ was observed from the argon-hydrogen plasma having Ar^+ catalyst and hydrogen, but not from argon alone. The sharp peaks in the spectrum were assigned to Ar II.

Detection of Fractional Rydberg State Molecular Hydrogen $\mathbf{H_2(1/4)}$. The observation of emission due to the reaction $H(1/4)+H^+ \rightarrow H_2(1/4)^+$ at low pressure (< 1 Torr) shown in Figures 1 and 2 indicates that $H(1/4)$ formed in the argon-hydrogen plasma. Molecular formation was anticipated under high-pressure conditions (~760 Torr). Thus, EUV spectroscopy of argon-hydrogen plasmas was performed to search for $H_2(1/4)$ from $H(1/4)$ formed by Ar^+ as a catalyst using a 15 keV electron beam to maintain the plasma and to collisionally excite vibration-rotational states of $H_2(1/4)$. The corresponding emission provides a direct measure of the internuclear distance; thus, this method provides the possibility of direct confirmation of $H_2(1/4)$.

The 100-350 nm spectrum of a 450 Torr plasma of argon containing about 1% hydrogen is shown in Figure 5. Lyman α was observed at 121.6 nm with an adjoining H_2 band, the third continuum of Ar was observed at 200 nm, O I was observed at 130.6 nm, and the $OH(A-X)$ band was observed at 309.7 nm. A series of sharp, evenly-spaced lines was observed in the region 145-185 nm. The only possibilities for peaks of the instrument width are those due to rotation or electronic emission from atoms or ions. The

series was not observed when krypton replaced argon or with any of the controls and could not be assigned to any known species [28].

The series matched the P branch of $H_2(1/4)$ for the vibrational transition $\upsilon = 1 \rightarrow \upsilon = 0$. P(1), P(2), P(3), P(4), P(5), and P(6) were observed at 155.0 nm, 160.2 nm, 165.8 nm, 171.1 nm, 178.0 nm, and 183.2 nm, respectively. The sharp peak at 147.3 nm may be the first member of the R branch, R(0). Since the vibration-rotational transitions of $H_2(1/4)$ are allowed with nuclear spin-rotational coupling, the vibrational rotational spectrum of $H_2(1/4)$ was predicted to comprise only the R(0) line and the P branch [28] in agreement with observations. The slope of a linear curve fit was 0.241 eV with an intercept of 8.21 eV which matches Eq. (10) very well for $p = 4$. Using Eqs. (6) and (7) with the measured rotational energy spacing of 0.24 eV establishes an internuclear distance of 1/4 that of the ordinary hydrogen species for $H_2(1/4)$. This technique which is the best measure of the bond distance of any diatomic molecule identifies and unequivocally confirms $H_2(1/4)$.

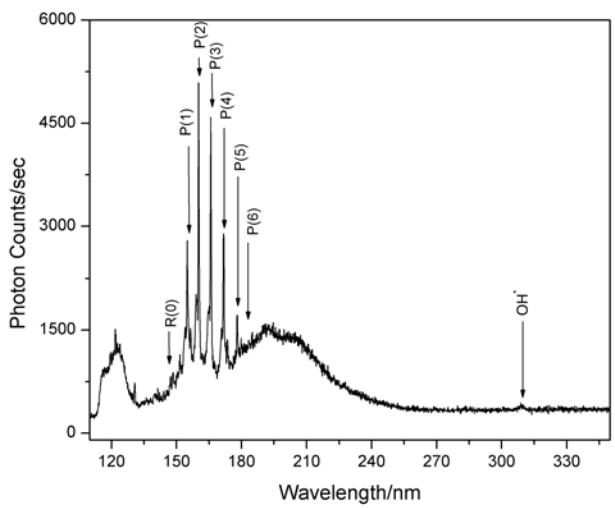

Figure 5. The 100-350 nm spectrum of a 450 Torr plasma of argon containing about 1% hydrogen and trace oxygen using a 15 keV electron gun. Lyman α was observed at 121.6 nm with an adjoining H_2 band, the third continuum of Ar was observed at 200 nm, O I was observed at 130.6 nm, and the $OH(A-X)$ band was observed at 309.7 nm. A series of sharp, evenly-spaced lines was observed in the region 145-185 nm. The series matched the P branch of $H_2(1/4)$ for the vibrational transition $\upsilon = 1 \rightarrow \upsilon = 0$. P(1), P(2), P(3), P(4), P(5), and P(6) were observed at 155.0 nm, 160.2 nm, 165.8 nm, 171.1 nm, 178.0 nm, and 183.2 nm, respectively. The sharp peak at 147.3 nm may be the first member of the R branch, R(0). The slope of a linear curve fit is 0.241 eV with an intercept of 8.21 eV which matches Eq. (10) very well for $p = 4$.

The Ar^+ catalyst mechanism was confirmed by atmospheric-pressure-plasma-gas flow at 75 sccm and nonflow conditions. Flow does not change known atomic and ionic line emission such as the O I line at 130.6 nm. In contrast, the series assigned to vibration-rotation of $H_2(1/4)$ was observed under static conditions; whereas, the series decreased to about 10% with flow indicating a reaction involving the formation of intermediates as predicted.

A possible confirmation of the lines identified in this study has been published previously. Ulrich, Wieser, and Murnick [42] compared the third continuum of argon gas with a very pure gas and a spectrum in which the gas was slightly contaminated by oxygen as evidenced by the second order of the 130 nm resonance lines at 160 nm. A series of very narrow lines at the instrument width having an intensity profile that was characteristic of that of a P-branch were observed in the 145-185 nm region. These lines shown in Figure 6 of Ref. [42] matched those in Figure 5. The slope of the linear curve fit was 0.24 eV with an intercept of 8.24 eV which matches Eq. (10) very well for $p = 4$. The series matches the predicted $\upsilon = 1 \rightarrow \upsilon = 0$ vibrational energy of $H_2(1/4)$ of 8.25 eV (Eq. (5)) and its predicted rotational energy spacing of 0.24 eV (Eq. (6)) with $\Delta J = +1; J = 1,2,3,4,5,6$ and $\Delta J = -1; J = 0$ where J is the rotational quantum number of the final state. With this assignment all of the peaks in Figure 6 of Ref. [42] could be identified; whereas, the evenly-spaced lines could not be unambiguously assigned by Ulrich et al [42]. The series was not observed in krypton and xenon plasmas. The determination of the presence of the common contaminant, hydrogen, in the argon plasmas is warranted in future studies.

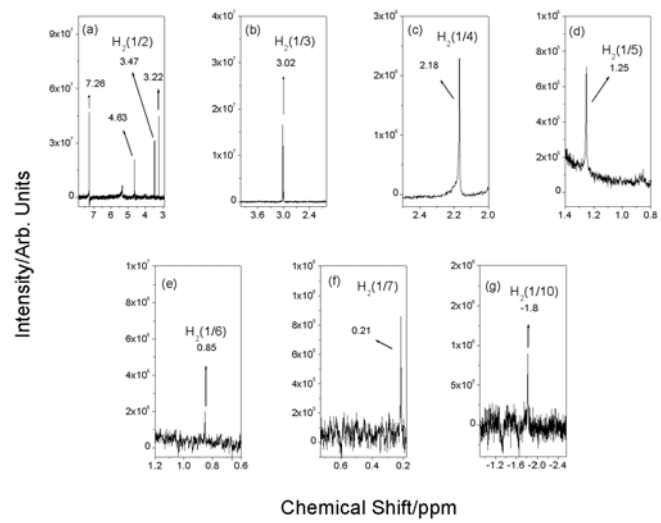

Figure 6 (a)-(g). ^1H NMR spectra on sealed samples of liquid-nitrogen-condensable helium-hydrogen plasma gases dissolved in $CDCl_3$ relative to tetramethylsilane (TMS). The solvent peak was observed at 7.26 ppm, the H_2 peak was observed at 4.63 ppm, and a singlet at 3.22 ppm matched silane. Singlet peaks upfield of H_2 were observed at 3.47, 3.02, 2.18, 1.25, 0.85, 0.21, and -1.8 ppm relative to TMS corresponding to solvent-corrected absolute resonance shifts of -29.16, -29.61, -30.45, -31.38, -31.78, -32.42, and -34.43 ppm, respectively. Using Eq. (12), the data indicates that p = 2, 3, 4, 5, 6, 7, and 10, respectively. The data matched the series $H_2(1/2)$, $H_2(1/3)$, $H_2(1/4)$, $H_2(1/5)$, $H_2(1/6)$, $H_2(1/7)$, and $H_2(1/10)$.

Isolation and Characterization of $H_2(1/p)$. *Cryotrap Pressure* Helium-hydrogen (90/10%) gas was flowed through the microwave tube and the cryosystem for 2 hours with the trap cooled to LN temperature. No change in pressure over time was observed when the dewar was removed, and the system was warmed to room temperature. The experiment was repeated under the same

conditions but with a plasma maintained with 60 W forward microwave power and 10 W reflected. In contrast to the control case, a liquid-nitrogen-condensable gas was generated in the helium-hydrogen plasma reaction since the pressure due to the reaction product rose from 10^{-5} Torr to 3 Torr as the cryotrap warmed to room temperature.

Mass Spectroscopy. The mass spectrum for the gases collected in the cryotrap from the He/H_2 (90/10%) plasma over the range $m/e=1$ to $m/e=200$ showed that the LN-condensable gas was highly pure hydrogen. The mass spectrum ($m/e=1$ to $m/e=200$) for the gases collected in the cryo-cooler from the He/H_2 (90/10%) plasma only showed peaks in the ($m/e=1$ to $m/e=50$) region. The $m/e=2$ peak was 40-50 times more intense than the $m/e=28$ (nitrogen), $m/e=32$ (oxygen), and $m/e=40$ (argon) peaks that were assigned to very trace residual air contamination. Whereas, without the plasma, the mass $m/e=2$ peak was present in only trace concentration ($\sim 10^{-10}$ Torr) compared with the air contaminant gases that were also present in low abundance ($\sim 10^{-9}$ Torr). Von Engel [43] gives the efficiency of production of various common ions at 70 eV and shows that the cross section for the formation of H_2^+ is 10% of that of air contaminants at the same partial pressure. Thus, hydrogen was ~500 times more abundant in the collected gas than air contaminants which may have originated through back-streaming in the mass spectrometer.

From the phase diagram of helium and hydrogen plotted from data given by Lide [44] and extended to lower pressures and temperatures using the Clausius-Clapeyron equation [45], it is not possible to condense ordinary hydrogen below ~50 Torr at 12-17 K. The condensation of a $m/e=2$ gas in the temperature range of 12-17 K at 700 mTorr that was not removed at 10^{-5} Torr indicates that a novel hydrogen gas formed in the plasma reaction between hydrogen and helium. The results are even more dramatic in the case of the condensation of a $m/e=2$ gas in the temperature range of 77 K using the LN cryotrap.

^1H NMR. The ^1H NMR on $CDCl_3$ showed only a singlet solvent ($CHCl_3$) peak at 7.26 ppm relative to tetramethylsilane (TMS) with small ^{13}C side bands. The ^1H NMR on ultrahigh purity hydrogen dissolved in $CDCl_3$ relative to tetramethylsilane (TMS) showed only singlet peaks at 7.26, 4.63, and 1.57 ppm corresponding to $CHCl_3$, H_2, and H_2O, respectively. The chemical shifts of the $CHCl_3$ and H_2O peaks matched the literature values of 1.56 and 7.26 ppm, respectively [46]. The error in the observed peaks was determined to be ± 0.01 ppm. The ^1H NMR spectroscopic results of the control prepared from the reagent helium-hydrogen mixture was the same as that of the high purity hydrogen control.

H_2 has been characterized by gas phase ^1H NMR. The experimental absolute resonance shift of gas-phase TMS relative to the proton's gyromagnetic frequency is -28.5 ppm [47]. H_2 was observed at 0.48 ppm compared to gas phase TMS set at 0.00 ppm [48]. Thus, the corresponding absolute H_2 gas-phase resonance shift of -28.0 ppm (-28.5 + 0.48) ppm was in excellent agreement with the predicted absolute gas-phase shift of -28.01 ppm given by Eq. (12).

The absolute H_2 gas-phase shift can be used to determine the solvent shift for H_2 dissolved in $CDCl_3$. The correction for the solvent shift can then be applied to other peaks to determine the gas-phase absolute shifts to compare to Eq. (12). The shifts of all of the peaks were relative to liquid-phase TMS which has an experimental absolute resonance shift of -31.5 ppm relative to the proton's gyromagnetic frequency [39, 40]. Thus, the experimental shift of H_2 in $CDCl_3$ of 4.63 ppm relative to liquid-phase TMS corresponds to an absolute resonance shift of -26.87 ppm (-31.5 ppm + 4.63 ppm). Using the absolute H_2 gas-phase resonance shift of -28.0 ppm corresponding to 3.5 ppm (-28.0 ppm - 31.5 ppm) relative to liquid TMS, the $CDCl_3$ solvent effect is 1.13 ppm (4.63 ppm - 3.5 ppm) which is comparable to that of hydrocarbons [46].

^1H NMR spectra on sealed samples of condensable helium-hydrogen plasma gases dissolved in $CDCl_3$ relative to tetramethylsilane (TMS) are shown in Figures 6 (a)-(f). The solvent peak was observed at 7.26 ppm, the H_2 peak was observed at 4.63 ppm, and a singlet at 3.22 ppm matched silane. Small ^{29}Si side bands were observed for the latter. The source was determined to be hydrogen-plasma reduction of the quartz tube. The peak was unchanged after three weeks at room temperature. No other silanes, silane decomposition species, or solvent decomposition species were observed even after one month of repeat NMR analysis. Since the plasma gases were first passed through an LN trap before the plasma cell, and the cryotrap was high-vacuum (10^{-6} Torr) capable, no hydrocarbons were anticipated. This was confirmed by mass spectroscopic and FTIR analysis that showed only water vapor in addition to silane as contaminants. Again, the source was determined to be hydrogen-plasma reduction of the quartz tube.

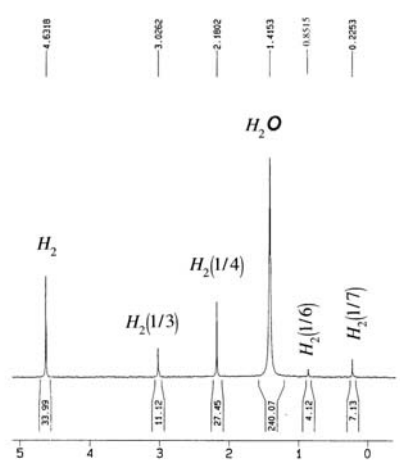

Figure 7. The ^1H NMR spectrum recorded at China Lake on gases from the thermal decomposition of $KH*I$ dissolved in $CDCl_3$ relative to tetramethylsilane (TMS). H_2 and H_2O were observed at 4.63 ppm and 1.42, respectively. Singlet peaks upfield of H_2 were observed at 3.02, 2.18, 0.85, and 0.22 ppm relative to TMS corresponding to solvent-corrected absolute resonance shifts of -29.61, -30.45, -31.78, and -32.41 ppm, respectively. Using Eq. (12),

the data indicates that p = 3, 4, 6, and 7, respectively. The data matched the series $H_2(1/3)$, $H_2(1/4)$, $H_2(1/6)$, and $H_2(1/7)$.

As further shown in Figures 6 (a)-(g), singlet peaks upfield of H_2 were observed at 3.47, 3.02, 2.18, 1.25, 0.85, 0.21, and -1.8 ppm relative to TMS corresponding to solvent-corrected absolute resonance shifts of -29.16, -29.61, -30.45, -31.38, -31.78, -32.42, and -34.43 ppm, respectively. Using Eq. (12), the data indicates that p = 2, 3, 4, 5, 6, 7, and 10, respectively. The data matched the series $H_2(1/2)$, $H_2(1/3)$, $H_2(1/4)$, $H_2(1/5)$, $H_2(1/6)$, $H_2(1/7)$, and $H_2(1/10)$. The molecules corresponding to the reaction product atom $H(1/3)$ with products from further transitions as given in Refs. [2-3] are in agreement with the observed molecules.

^1H NMR spectra were recorded at China Lake and at BlackLight Power, Inc. on ultrahigh purity hydrogen and gases from the thermal decomposition of $KH*I$ dissolved in $CDCl_3$ relative to tetramethylsilane (TMS). These samples were determined not to contain hydrocarbons by mass spectroscopy and FTIR analysis. Only the $CDCl_3$, H_2, and H_2O peaks were observed from the controls. As shown in Figure 7, novel singlet peaks upfield of H_2 were observed from a $KH*I$ -derived sample run at China Lake. The peaks at 3.02, 2.18, 0.85, and 0.22 ppm relative to TMS corresponded to solvent-corrected absolute resonance shifts of -29.61, -30.45, -31.78, and -32.41 ppm, respectively. Using Eq. (12), the data indicates that p = 3, 4, 6, and 7, respectively. The data matched the series $H_2(1/3)$, $H_2(1/4)$, $H_2(1/6)$, and $H_2(1/7)$. The observed products were consistent with those anticipated with the catalysis of *H* by *K* to form $H(1/4)$ and subsequent transition reactions [2-3, 8, 17, 20].

As shown in Figures 6 and 7, the observation of the series of singlet peaks upfield of H_2 with a predicted integer spacing of 0.64 ppm at 3.47, 3.02, 2.18, 1.25, 0.85, and 0.22 ppm identified as the consecutive series $H_2(1/2)$, $H_2(1/3)$, $H_2(1/4)$, $H_2(1/5)$, $H_2(1/6)$, and $H_2(1/7)$ and $H_2(1/10)$ at -1.8 ppm provides powerful confirmation of the existence of $H_2(1/p)$. Furthermore, the ^1H NMR spectra of gases from the thermal decomposition of $KH*I$ matched those of LN-condensable hydrogen. This provides strong support that compounds such as $KH*I$ contain hydride ions $H^-(1/p)$ in the same fractional quantum state p as the corresponding observed $H_2(1/p)$. Observational agreement with predicted positions of upfield-shifted ^1H MAS NMR peaks (Eq. (13)) of the compounds [8, 20, 30-32], catalyst reactions [17, 20, 23-24], and spectroscopic data [17] supports this conclusion.

The existence of novel alkaline and alkaline earth hydride and halido-hydrides were previously identified by large distinct upfield ^1H NMR resonances compared to the NMR peaks of the corresponding ordinary hydrides [20, 30-32]. Using a number of analytical techniques such as XPS and time-of-flight-secondary-mass-spectroscopy (ToF-SIMS) as well as NMR, the hydrogen content was assigned to $H^-(1/p)$, novel high-binding-energy hydride ions in stable fractional principal quantum states [8, 20, 30-32]. Upfield shifts of the novel hydride compounds matched those predicted for $H^-(1/2)$ and $H^-(1/4)$ (Eq. (13)). Novel spectral emission from $H^-(1/2)$ and $H^-(1/2)$, the predicted products from the potassium catalyst reaction and the supporting results of 1.) the formation of a hydrogen plasma with intense extreme ultraviolet (EUV) emission at low temperatures (e.g. $\approx 10^3\,K$) and an extraordinary low field strength of about 1-2 V/cm [9-12, 17-24] or without an electric field or power input other than thermal [21-22] from atomic hydrogen and certain atomized elements or certain gaseous ions that serve as catalysts, 2.) a high positive net enthalpy of reaction [20], 3.) characteristic predicted catalyst emission [17, 23-24], 4.) ~15 eV Doppler broadening of the Balmer lines [17, 23-24], and 5.) inversion of the Lyman lines [23-24] have also been reported previously.

Based on their stability characteristics, advanced hydride technologies are indicated. Hydride ions $H^-(1/p)$ having extraordinary binding energies may stabilize a cation M^{x+} in an extraordinarily high oxidation state as the basis of a high voltage battery. And, a rocketry propellant based on $H^-(1/24)$ to $H_2(1/24)$ may be possible with an energy release so large that it may be transformational. Significant applications also exist for the corresponding molecular species $H_2(1/p)$. The results of this study indicate that excited vibration-rotational levels of $H_2(1/4)$ could be the basis of a UV laser that could significantly advance photolithography.

Power Balance of the Helium-Hydrogen Microwave Plasma In addition to high energy spectral emission as shown in Sec. IIIA and previously [1-5], other indications of very energetic reactions are observed. For example, population inversion has been observed from plasmas which contain atomic hydrogen with the presence of a catalyst [23-26], and selective H broadening with a microwave plasma having no high DC field present was reported previously [13-15]. Microwave He/H_2 and Ar/H_2 plasmas showed extraordinary broadening corresponding to an average hydrogen atom temperature of $80-120eV$ and $110-130eV$, respectively. Whereas, pure hydrogen and Xe/H_2 microwave plasmas showed no excessive broadening corresponding to an average hydrogen atom temperature of <2 eV [13-15]. Only the H lines were Doppler broadened, and this result was shown to be inexplicable by any mechanism based on electric field acceleration of charged species. The observation of excessive Balmer line broadening in microwave driven plasmas as well as other hydrogen-mixed plasmas maintained in glow discharge [10-15] and RF discharge cells [14, 16] as well as unique chemically driven plasmas called resonant-transfer or rt-plasmas [17, 20, 23-24] requires a source of energy other than that provided by the electric field. The formation of fast H only in specific predicted plasmas was explained by a resonant energy transfer between hydrogen atoms and catalysts such as Ar^+ or He^+ of an integer multiple of the potential energy of atomic hydrogen, 27.2 eV [13-15]. Consistent with predictions, noncatalyst plasma mixtures such as Kr/H_2 and Xe/H_2 show no unique features. The observation of the $H_2(1/4)$ rotational lines reported in Sec. IIIAb from Ar/H_2 plasmas but not from Kr/H_2 and Xe/H_2 plasmas also matches predictions.

The excess power of the catalytic reaction was measured by water bath calorimetry. The water bath calorimeter is an absolute standard and indicated $P_{in} = 41.9 \pm 1W$ input power at the selected diode settings for all control plasmas. From these results, power input to the helium-hydrogen plasma was confidently known as the diode readings were identically matched for the controls. For

example, the *T(t)* water bath response to stirring and then with selected panel meter readings of the constant forward and reflected microwave input power to krypton was recorded. Using the corresponding $\dot{T}(t)$ in Eq. (17), the microwave input power was determined to be 41.9 ± 1 W. The *T(t)* response was significantly increased for helium-hydrogen (95/5%). From the difference in the *T(t)* water bath response, the output and excess power of the helium-hydrogen plasma reaction was determined to be 62.1 ± 1 W and 20.2 ± 1 W using Eq. (17) and Eq. (16) with the measured $P_{in} = 41.9 \pm 1W$. The sources of error were the error in the calibration curve (± 0.05 W) and the measured microwave input power (± 1 W). The propagated error of the calibration and power measurements was ± 1 W. Given an excess power of 20.2 W in 3 cm^3 and a helium-hydrogen (95/5%) flow rate of 10.0 sccm, the excess power density and energy balance were high, 6.7 W/cm^3 and -5.4×10^4 *kJ/mole* H_2 (280 *eV / H atom*), respectively.

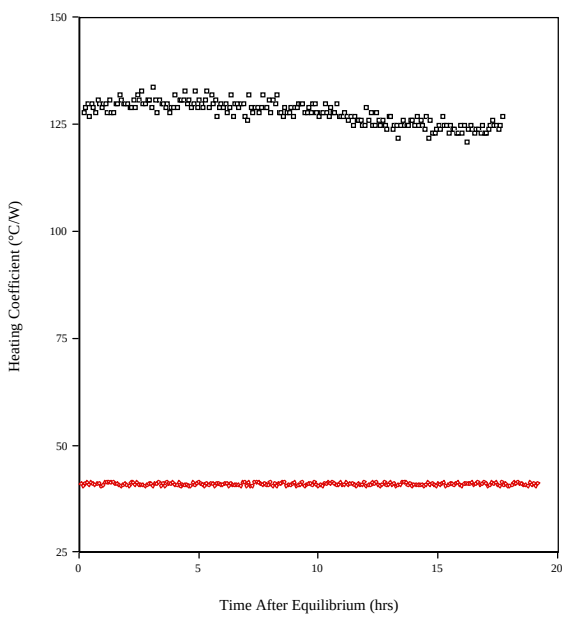

Figure 8. Plot of the heating coefficients versus time. (top) - K_2CO_3 electrolysis with a nickel wire cathode at 83.0 mA and 1.95 V, (bottom) - resistor working in K_2CO_3. The heating coefficient of the heater run (calibration) was 41°C/W.; whereas, the heating coefficient of the electrolysis run was 127 °C/W. The production of excess power of 81.8 mW was observed that was 3.1 times P_{cell} and 75% of P_{appl}.

Isolation and Characterization of $H_2(1/p)$ from Electrolysis Cells. ***Power Balance of the Electrolysis Cells.*** The temperature versus time results of the electrolysis of K_2CO_3 with a nickel wire cathode at 83.0 mA constant current and 1.95 V corresponding to an electrolysis resistive input power, P_{cell}, of 39.0 mW (Eq. (22)) and heater run of K_2CO_3 with 50 mW appear in Figure 8. The heating coefficient of the heater run (calibration) was 41°C/W.; whereas, the heating coefficient of the electrolysis run was 127°C/W. The production of excess enthalpy is observed. The higher the heating coefficient, the more heat released in the process. Using Eq. (31), the excess power, Q_{xs}, was determined to be

$$Q_{xs} = P_{cell}\left(\frac{a_1}{a_2} - 1\right) = 39.0\,\mathrm{mW}\left(\frac{127}{41} - 1\right) = 81.8\,\mathrm{mW} \qquad (34)$$

Thus, the experiment developed an extra 81.8 mW over the input power, P_{cell}, which corresponded to a total thermal power of 3.1 times P_{cell} and 75% of P_{appl}. The Faradaic efficiency of the production of gas by a K_2CO_3 cell and a control Na_2CO_3 cell was 100% within experimental error. The results of excess heat observed only from the K_2CO_3 cell could not be explained by recombination of electrolysis gases as shown previously [49, 50]. The observed heating coefficient of the electrolysis run when Na_2CO_3 replaced K_2CO_3 was 45 °C/W; whereas, the heating coefficient of the heater run (calibration) was 46 °C/W. The production of excess heat was not observed for the control as predicted. Similar excess heat results from K_2CO_3 electrolysis have been reported by Mills [49-51] and others [50, 52].

Neglect, for the moment that $H(1/2)$ can form a diatomic molecule $H_2(1/2)$ and subsequent transitions to lower energy states occur to a substantial extent. From Eqs. (1a) and (1b), 40.8 eV is released per H atom transition to the n = 1/2 quantum state due to catalysis by potassium ions which corresponds to 8 MJ/mole of H_2 [9, 17, 19-20]. In contrast, only 286 kJ is consumed by electrolyzing one mole of H_2O to produce one mole of H_2 (Eq. (15)). Thus, the excess power of 82 mW produced by the K_2CO_3 electrolytic cell as shown in Figure 8 (which also produces 0.43 μmoles of H_2 per second) could be accounted for by the conversion of at most 3.5% of the hydrogen atoms from the n = 1 state to the n = 1/2 state.

^1H *NMR of Electrolysis Gases.* ^1H NMR spectra on sealed samples of K_2CO_3 electrolytic gases dissolved in $CDCl_3$ relative to tetramethylsilane (TMS) are shown in Figures 9 (a)-(d). The solvent peak was observed at 7.26 ppm, the H_2 peak was observed at 4.63 ppm. No hydrocarbons were anticipated to permeate the nickel tube. This was confirmed by mass spectroscopic and FTIR analysis. For example, the FTIR spectra of the electrolysis gases in the region of the C-H stretching showed no evidence for hydrocarbons. As further shown in Figures 9 (a)-(d), singlet peaks upfield of H_2 were observed at 3.49[1], 2.17, 1.25, 0.86, and 0.21 ppm relative to TMS corresponding to solvent-corrected absolute resonance shifts of -29.14, -30.46, -31.38, -31.77, -and -32.42 ppm, respectively. Using Eq. (12), the data indicates that p = 2, 4, 5, 6, and 7, respectively.

The observed series has implications for the catalysis reactions and the corresponding rates of the formation of atoms $H(1/p)$ and the corresponding molecules $H_2(1/p)$ and their diffusion through the nickel tubing. The product of the catalysis of H by potassium ions is $H(1/2)$ corresponding to the peak at 3.49 ppm shown in Figure 9. Similarly, the product of catalysis of H by K is $H(1/4)$ corresponding to the peak at 2.17 ppm shown in Figure 9 which was the dominant peak. K as the principle catalyst with K_2CO_3 or

[1] The broad increase in the baseline in the region 3.25-3.75 ppm was an instrument artifact.

$K(m)$ as the source was also supported by the observation of characteristic catalyst emission and EUV emission from the corresponding hydride ion having an upfield-shifted ^1H MAS NMR peak at -4.4 ppm as discussed in Sec. IB. Since the products of the catalysis reaction have binding energies of $m \cdot 27.2eV$, they may further serve as catalysts by so called exothermic disproportionation reactions where one atom goes to a lower state (e.g. $n = \frac{1}{2} \rightarrow \frac{1}{3}, \frac{1}{3} \rightarrow \frac{1}{4}, \frac{1}{4} \rightarrow \frac{1}{5},$) while another goes to a higher state [2, 3, 7]. Thus, $H_2(1/p)$ molecules corresponding to the product atoms $H(1/p)$ from further transitions having $p > 2$ or $p > 4$ as given in Refs. [2-3] are anticipated as the reaction products.

As shown in Figures 9 (a)-(d), the observation of the series of singlet peaks upfield at 3.49, 2.17, 1.25, 0.86, and 0.21 ppm with an integer spacing of 0.64 ppm (except for the previously observed 3.02 peak shown in Figure 6) identified as the consecutive series $H_2(1/2)$, $H_2(1/4)$, $H_2(1/5)$, $H_2(1/6)$, and $H_2(1/7)$ provides powerful confirmation of the existence of $H_2(1/p)$.

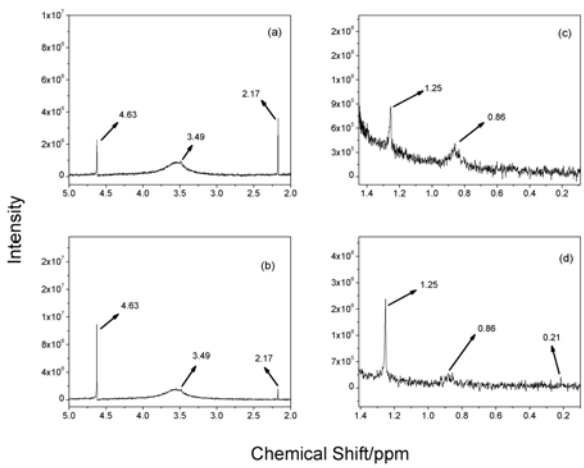

Figure 9. (a)-(d). ^1H NMR spectra on sealed samples of K_2CO_3 electrolytic gases dissolved in $CDCl_3$ relative to tetramethylsilane (TMS). The solvent peak was observed at 7.26 ppm, and the H_2 peak was observed at 4.63 ppm. Singlet peaks upfield of H_2 were observed at 3.49, 2.17, 1.25, 0.86, and 0.21 ppm relative to TMS corresponding to solvent-corrected absolute resonance shifts of -29.14, -30.46, -31.38, -31.77, and -32.42 ppm, respectively. Using Eq. (12), the data indicates that p = 2, 4, 5, 6, and 7, respectively. The data matched the series $H_2(1/2)$, $H_2(1/4)$, $H_2(1/5)$, $H_2(1/6)$, and $H_2(1/7)$.

Mass Spectroscopy of Electrolysis Gases. $H_2(1/2)$ was identified by mass spectroscopy as a species with a mass to charge ratio of two ($m/e = 2$) that has a higher ionization potential than that of normal hydrogen by recording the ion current as a function of the electron gun energy. The mass spectra of the K_2CO_3 and Na_2CO_3 electrolysis gases was obtained over the range $m/e = 1$ to $m/e = 200$. In both cases, the sample contained only hydrogen.

The relative changes in the $m/e = 2$ ion current while changing the electron gun energy from 30 to 70 eV indicated that the K_2CO_3 electrolysis gases has a higher ionization potential than ultrapure hydrogen and Na_2CO_3 electrolysis gases. Upon increasing the ionization potential from 30 eV to 70 eV, the $m/e = 2$ ion current for the controls increased by a factor of about 30%; whereas, the current for K_2CO_3 electrolysis gases collected under liquid nitrogen increased by a factor of about 10 under the same pressure condition as that of the controls.

Conclusion

In this study we made specific theoretical predictions regarding the exothermic reaction to form $H_2(1/p)$ and its characterization and tested them with standard, easily interpretable experiments. The results show that new states of hydrogen are formed by reaction of hydrogen atoms with He^+, Ar^+, and potassium ions and atoms that serve as catalysts but not with control atoms and ions as predicted. The observation of excess enthalpy and the same states of hydrogen, $H_2(1/p)$, from chemicals compound, plasma gases, and electrolysis cells demonstrates the hydrogen catalysis reaction occurs in liquid-solid interfacial environments as well as in the gas phase under a range of reaction conditions. The power results indicate that a new power source based on the catalysis of atomic hydrogen is not only possible, but it may be competitive with gas-turbine combustion. Furthermore, since the identified $H_2(1/p)$ byproduct is stable and lighter-than-air, it can not accumulate in the Earth's atmosphere. The environmental impact of handling fossil fuels and managing the pollution of air, water, and ground caused by the ash generated by fossil fuels or the radioactive waste from a nuclear plant may be eliminated.

Acknowledgments. Special thanks to D. E. Murnick and M. Salvermoser of Rutgers University for providing the 15 keV electron gun. D. C. Harris, Naval Air Warfare Center Weapons Division, Naval Air Warfare Center, China Lake, CA, is acknowledged for suggesting the method of identifying $H_2(1/p)$ by ^1H NMR using $CDCl_3$ solvent. D. C. Harris and L. Merwin are acknowledged for preparing and analyzing a $KH*I$ NMR sample.

References

(1) R. L. Mills, P. Ray, *J. Phys. D: Appl. Phys.*, **2003**, *36*, 1535.
(2) R. L. Mills, P. Ray, B. Dhandapani, M. Nansteel, X. Chen, J. He, *J Mol. Struct.*, **2002**, *643* (1-3), 43.
(3) R. Mills, P. Ray, *Int. J. Hydrogen Energy*, **2002**, *27*, 301.
(4) R. L. Mills, P. Ray, J. Dong, M. Nansteel, B. Dhandapani, J. He, *Vib. Spectrosc.*, **2003**, *31*, 195.
(5) R. Mills, P. Ray, *Int. J. Hydrogen Energy*, **2002**, *27*, 533.
(6) R. Brunch, P L. Altick, E. Trabert, P. H. Heckmann, *J. Phys. B: At. Mol. Phys.*, **1984**, *17*, L655.
(7) R. Mills, *The Grand Unified Theory of Classical Quantum Mechanics*, September 2001 Edition, BlackLight Power, Inc., Cranbury, New Jersey, Distributed by Amazon.com; January (2003) Edition posted at www.blacklightpower.com.
(8) R. L. Mills, "The Nature of the Chemical Bond Revisited and an Alternative Maxwellian Approach," submitted.
(9) R. Mills, J. Dong, Y. Lu, *Int. J. Hydrogen Energy*, **2000**, *25*, 919.

(10) R. Mills, M. Nansteel, P. Ray, *IEEE Transactions on Plasma Science*, **2002**, *30*, 639.
(11) R. Mills, M. Nansteel, P. Ray, *New J. Phys*., **2002**, *4*, 70.1.
(12) R. Mills, M. Nansteel, P. Ray, *J. Plasma Phy.s*, **2003**, *69*, 131.
(13) R. L. Mills, P. Ray, B. Dhandapani, R. M. Mayo, J. He, *J. Appl. Phys*., **2002**, *92*, 7008.
(14) R. L. Mills, P. Ray, B. Dhandapani, J. He, *IEEE Trans. Plasma Sci*., **2003**, *31*(3), (2003), 338.
(15) R. L. Mills, P. Ray, *New J. Phys*., www.njp.org, **2002**, *4*, 22.1.
(16) J. Phillips, C. Chen, "Evidence of Energetic Reaction Between Helium and Hydrogen Species in RF Generated Plasmas," submitted.
(17) R. L. Mills, P. Ray, *Int. J. Hydrogen Energy*, **2003**, *28*, 825.
(18) R. Mills, Int. J. Hydrogen Energy, **2001**, *26*, 1041.
(19) R. Mills, P. Ray, *Int. J. Hydrogen Energy*, **2002**, *27*, 183.
(20) R. Mills, P. Ray, B. Dhandapani, W. Good, P. Jansson, M. Nansteel, J. He, A. Voigt, "Spectroscopic and NMR Identification of Novel Hydride Ions in Fractional Quantum Energy States Formed by an Exothermic Reaction of Atomic Hydrogen with Certain Catalysts," in press.
(21) H. Conrads, R. Mills, Th. Wrubel, *Plasma Sources Sci. Technol*., **2003**, *12*, 389.
(22) R. Mills, T. Onuma, Y. Lu, Int. J. Hydrogen Energy, **2001**, *26*, 749.
(23) R. Mills, P. Ray, R. M. Mayo, *IEEE Trans. Plasma Sci.*, **2003**, *31* (2), 236.
(24) R. L. Mills, P. Ray, *J. Phys. D: Appl. Phys*., **2003**, *36*, 1504.
(25) R. Mills, P. Ray, R. M. Mayo, *Appl. Phys. Lett*., **2003**, *82* (11), 1679.
(26) R. L. Mills, P. C. Ray, R. M. Mayo, M. Nansteel, B. Dhandapani, J. Phillips, "Spectroscopic Study of Unique Line Broadening and Inversion in Low Pressure Microwave Generated Water Plasmas," submitted.
(27) R. L. Mills, X. Chen, P. Ray, J. He, B. Dhandapani, *Thermochim. Acta*, **2003**, *406* (1-2) 35.
(28) R. L. Mills, Y. Lu, J. He, M. Nansteel, P. Ray, X. Chen, A. Voigt, B. Dhandapani, "Spectral Identification of New States of Hydrogen," submitted.
(29) R. Mills, B. Dhandapani, W. Good, J. He, "New States of Hydrogen Isolated from K_2CO_3 Electrolysis Gases,"submitted.
(30) R. Mills, B. Dhandapani, M. Nansteel, J. He, T. Shannon, A. Echezuria, *Int. J. Hydrogen Energy*, **2001**, *26*, 339.
(31) R. Mills, B. Dhandapani, N. Greenig, J. He, *Int. J. Hydrogen Energy*, **2000**, *25*, 1185.
(32) R. Mills, B. Dhandapani, M. Nansteel, J. He, A. Voigt, *Int. J. Hydrogen Energy*, **2001**, *26*, 965.
(33) R. Mills, E. Dayalan, P. Ray, B. Dhandapani, J. He, *Electrochim. Acta*, **2002**, *47*, 3909.
(34) M. Karplus, R. N. Porter, *Atoms and Molecules an Introduction for Students of Physical Chemistry*, The Benjamin/Cummings Publishing Company, Menlo Park, California, (1970), pp. 447-484.
(35) NIST Atomic Spectra Database, www.physics.nist.gov/cgi-bin/AtData/display.ksh.
(36) H. Beutler, *Z. Phys. Chem*., **1934**, *27B*, 287.
(37) G. Herzberg, L. L. Howe, *Can. J. Phys*., **1959**, *37*, 636.
(38) P. W. Atkins, *Physical Chemistry*, Second Edition, W. H. Freeman, San Francisco, (1982), p. 589.
(39) K. K. Baldridge, J. S. Siegel, *J. Phys. Chem. A*, **1999**, *103*, 4038.
(40) J. Mason, Editor, *Multinuclear NMR*, Plenum Press, New York, (1987), Chp. 3.
(41) J. Wieser, D. E. Murnick, A. Ulrich, H. A Higgins, A. Liddle, W. L. Brown, *Rev. Sci. Instrum.*, **1997**, *6* (3), 1360.
(42) A. Ulrich, J. Wieser, D. E. Murnick, Second International Conference on Atomic and Molecular Pulsed Lasers, *Proc. SPIE*, **1998**, *3403*, 300.
(43) A. von Engel, *Ionized Gases*, American Institute of Physics Press, New York, (1965), pp. 62-64.
(44) D. R. Lide, *CRC Handbook of Chemistry and Physics*, 76 th Edition, CRC Press, Boca Raton, Florida, (1995-6), p. 6-66 and p. 6-140.
(45) I. N. Levine, *Physical Chemistry*, McGraw-Hill Book Company, New York, (1978), pp. 174-175.
(46) H. E. Gottlieb, V. Kotlyar, A. Nudelman, *J. Org. Chem*., **1997**, *62*, 7512.
(47) C. Suarez, E. J. Nicholas, M. R. Bowman, J. Phys. Chem. A, **2003**, *107*, 3024.
(48) C. Suarez, "Gas-phase NMR spectroscopy," *The Chem. Educator*, 1998, 3 (2).
(49) R. Mills, W. Good, *Fusion Technol*., **1995**, *28*, 1697.
(50) R. Mills, W. Good, R. Shaubach, *Fusion Technol*., **1994**, *25*, 103.
(51) R. Mills, S. Kneizys, *Fusion Techno*l., **1991**, *20*, 65.
(52) J. Niedra, I. Meyers, G. C. Fralick, R. Baldwin, "Replication of the Apparent Excess Heat Effect in a Light Water-Potassium Carbonate-Nickel Electrolytic Cell," NASA Technical Memorandum 107167, February, (1996). pp. 1-20.; Niedra, J., Baldwin, R., Meyers, I., NASA Presentation of Light Water Electrolytic Tests, May 15, 1994.